Temporal evolution of age data under transient pumping conditions

Authors: Leray S. [1, *, #], de Dreuzy J.-R.[1, 2], Aquilina L.[1], Vergnaud-Ayraud V.[1], Labasque T.[1], Bour O.[1], Le Borgne T.[1].

[1] Géosciences Rennes (UMR 6118 CNRS), Université de Rennes 1, Campus de Beaulieu, 35042 Rennes cedex, France

[2] IDAEA (CSIC), c/ Jordi Girona, 08034, Barcelona, Spain

*Corresponding author: sarah.leray1@gmail.com

Now at: IFP Energies nouvelles, 1-4, avenue de Bois-Préau, 92852 Rueil-Malmaison, France

Key words: groundwater age, residence time distribution, environmental tracers, chlorofluorocarbons, heterogeneous aquifers, transient flow conditions

Abstract

While most age data derived from tracers have been analyzed in steady-state flow conditions, we determine their temporal evolution when starting a pumping. Our study is based on a model made up of a shallowly dipping aquifer overlain by a less permeable aquitard characteristic of the crystalline aquifer of Plœmeur (Brittany, France). Under a pseudo transient flow assumption (instantaneous shift between two steady-state flow fields), we solve the transport equation with a backward particle-tracking method and determine the temporal

evolution of the concentrations at the pumping well of CFC-11, CFC-12, CFC-113 and SF_6. Apparent ages evolve because of the modifications of the flow pattern and because of the non-linear evolution of the tracer atmospheric concentrations. To identify the respective role of these two causes, we propose two successive analyses. We first convolute residence time distributions initially arising at different times at the same sampling time. We secondly convolute one residence time distribution at various sampling times. We show that flow pattern modifications control the apparent ages evolution in the first pumping year when the residence time distribution is modified from a piston-like distribution to a much broader distribution. In the first pumping year, the apparent age evolution contains transient information that can be used to better constrain hydrogeological systems and slightly compensate for the small number of tracers. Later, the residence time distribution hardly evolves and apparent ages only evolve because of the tracer atmospheric concentrations. In this phase, apparent age time-series do not reflect any evolution in the flow pattern.

1. Introduction

Groundwater flow is by nature transient, because of the temporal variations of boundary conditions such as the variations of recharge over different time scales (seasons, decades, centuries or more) and because of anthropogenic forcings such as pumping or artificial recharge. Pumping has a significant impact on the flow pattern and on solute transport. They induce more convergent flow pattern and, even in some cases, some extension of recharge areas (Bredehoeft, 2002; Frind et al., 2005). It will as well speed up flows and modify the relative role of structures, hydrodynamic properties and boundary conditions – increasing for instance the effective recharge rate of unconfined aquifers in close connection to the surface (Leray et al., 2012; Sophocleous, 2005).

Environmental tracers have been widely used for water sources identification, estimation of residence time distribution and model calibration amongst others (Castro et al., 1998; Cook et al., 2005; Long and Putnam, 2009; McMahon et al., 2010; Stichler et al., 2008). Because they integrate velocities along flow paths, they reflect flow conditions over various time scales in the past. They are sensitive to transient phenomena affecting the flow field. More precisely, they are sensitive to transient phenomena occurring over time scales comparable to their characteristic time (Zuber et al., 2011).

Yet, the influence of transient flow conditions on environmental tracer concentration has hardly been addressed. Sanford et al. (2004) have reconstructed transient recharge rates using ^{14}C data in the regional alluvial middle Rio Grande Basin. Schwartz et al. (2010) have noticed that the interpretation of ^{14}C age in transient flow models can be ambiguous in terms of flow pattern as data distributed over the aquifer reflect different flow conditions. Long and Putnam (2009) have incorporated CFCs and ^{3}H data from a karstic system in binary mixing model with dilution allowing parameters to vary with time. Fewer studies have analyzed the role of transient flow conditions on residence time distribution. Using numerical simulations, Troldborg et al. (2008) have showed the effect of recharge seasonality on residence time distribution and have noticed distinct behaviors. In the shallowest part of the studied heterogeneous aquifer, residence times tend to be smaller than in steady-state flow conditions while they tend to be higher in the deepest part of the aquifer. The effect in a fully-penetrating well is however negligible. Zinn and Konikow (2007) have analyzed the effect of the start of pumping on a synthetic configuration composed of an aquifer overlain by an aquitard. Their study have revealed important changes of the mean residence time at the pumping well and of the residence time distribution over long periods of time. Changes only come from the

modification of the flow pattern as they solely focused on the mean residence time and not on the apparent ages obtained from tracers.

In this study, we determine the influence of the transient groundwater flow pattern induced by anthropogenic forcing on environmental tracers concentrations (CFC-11, CFC-12, CFC-113 and SF_6) interpreted in apparent ages. We consider that the transient flow pattern is induced by the instantaneous start of a pumping well. Tracer concentrations are reported at the pumping well. Our study is based on the hydrogeological setting of Plœmeur, which is a well documented aquifer where water has been produced for the last two decades for the water supply of the nearby city (Le Borgne et al., 2004; Le Borgne et al., 2006; Ruelleu et al., 2010; Touchard, 1999). Although based on a specific site, the results of this study can be generalized to shallowly dipping aquifers overlain by a leaking layer. Such condition has been proved to be of importance for groundwater resources in hard-rock aquifers (Leray et al., 2013). While our objective is more methodological than targeted to a specific site, the Plœmeur aquifer still offers a complex and yet realistic hydrodynamic context. We use hydrogeological models previously calibrated in steady-state flow conditions under pumping (Leray et al., 2012) and determine the effect of transient flow conditions on apparent ages. We first aim at determining the causes of the temporal evolution of the apparent ages and specifically when they rather come from the transient modifications of the flow pattern and when they are more linked to the specificities of the tracers, especially their atmospheric concentrations. We second aim at assessing the interest of age data time series for models segregation. After recalling in section 2 the hydrogeological, flow and transport models, we present the results in section 3 and discuss them in section 4.

2. Hydrogeological, flow and transport models

We successively describe the hydrogeological models of the Plœmeur site that will be used as a basis of this study, the flow and the transport models as well as the numerical methods used. We finally comment in details the derivation of the tracer concentrations and the corresponding apparent ages to highlight the possible causes of apparent age temporal variations.

2.1. Hydrogeological model

The study of the effects of transient flow conditions, induced by pumping, on age data is based on the Plœmeur aquifer, a highly heterogeneous hard-rock aquifer located on the south coast of Brittany near the city of Lorient (France). A previous study based on the inversion of gravimetric data has established a geological conceptual model (Ruelleu et al., 2010). This conceptual model is composed of two transmissive structures at large scale, the dipping contact zone and a North 20° normal fault, besides the Plœmeur and Guidel granites and overlying micaschists acting as a typical aquitard. Local heterogeneities are not represented in the model. The supplying area to the pumping well which amounts to a few square kilometers is limited in the North-South direction by these two granites. The pumping rate thus has a strong impact on flow pattern within this heterogeneous aquifer.

Because the shape and the dip of the contact zone are only partially known, the overall thickness of the aquitard-aquifer system remains relatively uncertain. To account for this uncertainty, a few structural models with distinct thickness have been built (Figure 1 and Table 1). The hydraulic properties of the different rocks have been set either to common values as for the granites which are found almost impervious (10^{-11} m/s), or to measured values as for the micaschists (10^{-7} m/s – $5x10^{-6}$ m/s) and the contact zone ($1.9x10^{-3}$ m^2/s –

$3x10^{-3}$ m^2/s). In addition, the potential recharge rate R has been estimated at 200 mm per year (Carn, 1990; Leray et al., 2012; Touchard, 1999). Following these constraints, each model has been calibrated against the mean piezometric level measured at the pumping well (-5.5 masl) in steady-state flow under pumping conditions (Leray et al., 2012) by slightly adjusting the contact zone transmissivity previously estimated from long-term pumping tests (Le Borgne et al., 2006). Uniform porosity has also been calibrated against the CFC-12 age (30 years ± 1 year in 2009). Note that the overall volume of the system is about $1.5x10^9$ m^3 and the mean residence time of the model – *i.e.* the first moment of the residence time distribution – is around 13 years in ambient conditions and 50 years in pumping conditions. .

Our study has been carried out on about ten representative hydrogeological models differing by their structure, their micaschists permeability and their porosity. The interest of considering different models is to investigate the potential influence of the hydrogeological structure on the apparent ages and their evolution. We discuss further in section 4 how this sensitivity might be useful as an additional way to characterize the flow pattern. Among this set of models, only two are used here to illustrate the methodology as they all lead to the same conclusions. Table 1 synthesizes the parameters of the two chosen hydrogeological models.

2.2. Flow model

Transient flow conditions are induced by starting a pumping well. The transient pumping rate $Q_w(t)$ is a step function going from zero before the starting date t_{switch}, to a positive value Q_p:

$$Q_w(t) = \begin{cases} 0 & t \leq t_{switch} \\ Q_p & t > t_{switch} \end{cases}. \qquad (1)$$

In the particular case of the site of Plœmeur, Q_p is set at 3.36×10^{-2} m^3/s. Pumping started in 1991 and the most part of the evolution of the piezometric levels occurred only in a few years after the start of pumping. t_{switch} has thus been set at 1994. We solve the 3D diffusivity equation for the hydraulic head $h(\boldsymbol{x}, t)$ with free surface boundary conditions under a pseudo transient flow approximation:

$$\nabla.(K(\boldsymbol{x})\nabla h(\boldsymbol{x},t)) = 0 \quad (2)$$

$$\left.\begin{array}{ll} K(\boldsymbol{x})\nabla h(\boldsymbol{x},t)\cdot\boldsymbol{n} = -R \quad \& \quad h(\boldsymbol{x},t) = z(\boldsymbol{x}) & \text{where } h < z_{ground} \\ h = z_{ground} & \text{anywhere else} \end{array}\right\} \text{ on } \Gamma_s \quad (3)$$

$$\nabla h(\boldsymbol{x})\cdot\boldsymbol{n} = 0 \qquad \text{on } \Gamma_{west} \text{ and } \Gamma_{east} \quad (4)$$

$$h(\boldsymbol{x}) = z_{ground} - z_0 \quad \text{on } \Gamma_{north} \text{ and } \Gamma_{south} \quad (5)$$

$$\int_{\Gamma_w} K(\boldsymbol{x})\nabla h(\boldsymbol{x},t)\cdot\boldsymbol{n_w}\, d\Gamma_w = Q_W(t) \quad \text{sink term} \quad (6)$$

where $K(\boldsymbol{x})$ is the hydraulic conductivity; $\boldsymbol{n}$ is the outgoing normal to the saturated domain; R is the potential recharge rate; z_{ground} is the ground surface elevation; Γ_s is the top of the saturated domain; Γ_{west}, Γ_{east}, Γ_{north} and Γ_{south} are respectively the West, East, North and South sides of the domain; z_0 is a reference height; $\boldsymbol{n}_w$ is the ingoing normal to the well screen; Γ_w is the well screen surface and $Q_w(t)$ is the transient pumping rate defined in equation 1 and located at $\boldsymbol{x}_w$. The pseudo transient approximation intervenes in equation 6 and consists in assuming that steady-state flow conditions are quickly established compared to the solute

transport evolution. This is a reasonable approximation of transient flow conditions valid at low specific storage and with the advantage of being less costly numerically. Practically, it consists in ignoring the transition between the two steady-state velocity fields under ambient and pumping conditions.

Equation 2 is solved in unconfined conditions since seepage conditions are *a priori* not known. Unconfined conditions are satisfied through both conditions at the free surface boundary of equation 3. When the free surface level is below the ground surface level, the effective recharge rate is equal to the potential recharge rate R; anywhere else, the free surface level is set at z_{ground} and the effective recharge rate continuously evolves from negative values in the discharge zone to positive potential recharge rate R. The model has been built to include the nearest watersheds both in ambient and pumping conditions in order to minimize the potential effects of the boundary conditions. No-flow conditions applied on the West and East boundaries (Equation 4, Figure 2) do not have any impact on the recharge areas captured by the pumping zone located at depth in the pumping well. Imposed heads, set at depth z_0 (5 meters below the ground surface level), are applied to the South and the North boundaries without any significant influence on the system because of the almost impervious granites (Equation 5, Figure 2).

2.3. Transport model

Transport is considered only advective as the macro-scale dispersion from local dispersion and diffusion is assumed to have a much smaller effect compared to the macro-scale dispersion induced by structural heterogeneity and sampling (LaBolle and Fogg, 2001). Transport is modeled by the advection equation (Bear, 1991; de Marsily, 1986):

$$\frac{\partial C(\boldsymbol{x},t)}{\partial t} + \nabla.\left(\frac{\boldsymbol{q}(\boldsymbol{x},\boldsymbol{t})}{\theta} C(\boldsymbol{x},t)\right) + \frac{Q_{\mathrm{W}}(t) C_{\mathrm{W}}(t)}{\theta} = 0 \qquad (7)$$

$$C(\boldsymbol{x}, t = 0) = C_0(\boldsymbol{x}) \qquad (8)$$

$$C(\boldsymbol{x},t) = C_1(t) \quad \text{on } \Gamma_1 \qquad (9)$$

with $C(\boldsymbol{x},t)$ the solute concentration at the position $\boldsymbol{x}$ and at the time t; θ the effective porosity; $Q_w(t)$ the rate of the pumping well; $C_w(t)$ the solute concentration at the pumping well; $C_0(\boldsymbol{x})$ the initial condition; $C_1(t)$ is the boundary condition on a first-type boundary (Γ_1) - such as the tracer atmospheric concentration at the free surface boundary - and $\boldsymbol{q}(\boldsymbol{x},t)$ the pseudo transient Darcy's flux derived from the head field $h(\boldsymbol{x},t)$:

$$\boldsymbol{q}(\boldsymbol{x},t) = -K(\boldsymbol{x})\nabla h(\boldsymbol{x},t). \qquad (10)$$

2.4. Numerical methods

The unconfined flow equations are solved using a computationally effective finite-volume approach with a local adaptation scheme (Bresciani et al., 2011). The advection equation is solved in backward-time that consists in reversing the flow field and adapting the boundary conditions (Neupauer and Wilson, 1999; Neupauer and Wilson, 2001; Neupauer and Wilson, 2002). To solve the transport equation, we use a Lagrangian random walk method well-suited to purely advective transport (de Dreuzy et al., 2007; Kinzelbach, 1988) and adapted to the unconfined conditions and to the backward-time resolution. We inject particles proportionally to flow (Kreft and Zuber, 1978) at the pumping well cell and tracked them to the aquifer free

surface. The chosen number of injected particles ($5x10^6$) is determined through a convergence test of the mean and the variance of the residence time distribution. Flow and transport simulations are carried out using the H2OLAB platform (Bresciani et al., 2011; Erhel et al., 2008; Erhel et al., 2009).

2.5. Computation and temporal evolution of apparent age

We derive the residence time distribution $p(t)$ from the equally likely residence times given by the particles. The mean concentration C_w of a tracer at the pumping well and at the sampling date t_w is determined by the convolution of the residence time distribution $p(t)$ with the atmospheric concentration $C_{in}(t_w - t)$ of the tracer (Kreft and Zuber, 1978; Maloszewski and Zuber, 1982):

$$C_w = \int_0^{+\infty} C_{in}(t_w - t)p(t)dt = \int_{-\infty}^{t_w} C_{in}(t)p(t_w - t)dt. \quad (11)$$

Note that, to highlight that the residence time distribution $p(t)$ is highly dependent on a given sampling date t_w, we later use it as $p(t_w - t)$ where $t_w - t$ represents the date at which water recharged, rather than as a function of the residence time "t" alone. Throughout the paper, $p(t_w - t)$ is named recharge date distribution. The apparent age A (Nir, 1964) of a tracer at the pumping well $\boldsymbol{x}_w$ and at the sampling date t_w is then obtained from the difference between t_w and the date at which the concentration C_w is equal to the atmospheric concentration:

$$A(t_w) = t_w - C_{in}^{-1}(C_w) = t_w - C_{in}^{-1}\left(\int_{-\infty}^{t_w} C_{in}(t)p(t_w - t)dt\right), \quad (12)$$

with C_{in}^{-1} the reciprocal function of the atmospheric concentration.

Equation 12 shows the two possible causes of the variation of age A with the sampling date t_w. The first cause is the evolution of the recharge date distribution $p(t_w - t)$ because of the modification of flow conditions that can be traced back to equation 1 through equations 2-11.

The shift from ambient to pumping conditions does not only change the flow magnitude but also the flow pattern, the recharge and discharge locations as well as the water mixing within the radius of action of the well (Bredehoeft, 2002). This first cause is solely linked to the flow conditions and does not depend on the tracer characteristics.

The second cause of the age variation directly comes from the tracer atmospheric concentration $C_{in}(t)$ through the convolution of equation 11. The non-linear temporal evolution of $C_{in}(t)$ modifies the sampling of the recharge date distribution $p(t_w - t)$. Monotonic and steep evolutions of $C_{in}(t)$ characteristic of the SF_6 and CFCs approximately between the 1970s and 1990s results in a large range of weights of the residence times in this period. Flatter evolutions characteristic of the CFCs after the early 1990s give a higher but more equilibrated contribution of the shorter residence times. Depending on the sampling date t_w, this equilibrated contribution is more or less significant. This effect occurs both in transient and steady-state flow conditions (Troldborg et al., 2008; Waugh et al., 2003; Zhang, 2004). Even under steady-state flow conditions, the non-linear evolution of the atmospheric concentration $C_{in}(t)$ lets the sampled concentration evolve. Under simpler terms, the evolution of the sampled concentration does not only come from the evolution of the system but also from the modification of the "observation device" (C_{in}).

It should be noted that this second effect is irrelevant when mixing is minimal like within the framework of the piston-flow model. In such cases, the residence time distribution resumes to a Dirac and the dependency to the tracer atmospheric concentration vanishes in equation 12 because of the direct transformation of C_{in} by C_{in}^{-1}. This effect is, however, very relevant

close to the aquifer discharge zones (springs, wells) where the mixing of flow paths is maximal. The mixing of sampled flow lines enhances the importance of the non-linear evolution of $C_{in}(t)$. The case studied here pertains more to this second situation, in which, finally, both the temporal evolutions of the recharge date distributions $p(t_w - t)$ and the tracer atmospheric concentration $C_{in}(t)$ can modify the sampled concentration and the derived age $A(t_w)$ (equation 12).

To analyze the temporal evolution of the apparent ages, we have determined them using equation 12 by convoluting the recharge date distributions $p(t_w - t)$ obtained under the pseudo transient conditions with the CFC-11, CFC-12, CFC-113 and SF_6 atmospheric concentrations at the evolving sampling dates t_w^i from 1994 to 2009 (Table 2). These dates correspond to sampling 0 to 15 years after the change of flow conditions from ambient to pumping conditions occurring at t_{switch} =1994.

3. Results

This section first reports the temporal evolution of the apparent ages at the pumping well for the hydrogeological model numbered 1 of the site of Plœmeur described in section 1 and in Table 1. It then analyses the respective effects of the modification of the flow pattern and of the evolution of the tracer atmospheric concentration. The implication of the temporal evolution of the apparent ages for models segregation is further discussed in section 4.1 by comparing the results of the models numbered 1 and numbered 2.

3.1. Temporal evolution of apparent age

Figure 3 shows the evolution of the apparent ages from CFC-11, CFC-12, CFC-113 and SF_6 concentrations with the sampling date t_w ranging from 1994 (ambient conditions) to 2009

(Table 2). At first sight, the apparent ages increase first sharply after the start of pumping and then more smoothly whatever the tracer. We indeed expect that the modifications of flow are maximal just after the start of the pumping and later decrease. Though similar, the apparent ages derived from the CFCs and SF_6 still exhibit some differences induced by the tracer atmospheric concentration $C_{in}(t)$. The temporal evolution is minimal for SF_6 because of the almost linear increase of its atmospheric concentration and maximal for the CFC-11 and CFC-12 because of the strong and non-monotonic variations of their atmospheric concentration (IAEA, 2006). CFC-11 and CFC-12 display similar variations because of the similar shapes of their atmospheric concentration chronicles.

The increase of the apparent ages in the models considered here is somehow counterintuitive. Indeed, in the exponential model (Haitjema, 1995), the residence time distribution is independent of the pumping rate. Besides, in the piston-flow model, as said in section 2.5, apparent ages remain constant whatever the sampling dates due to minimal mixing. When starting a pumping in those conditions, one would expect an increase of velocity that would directly reduce the residence time and then the apparent ages. In the more complex system modeled here, pumping has a nontrivial effect on the apparent ages. Further insight is given by the analysis of the recharge date distribution $p(t_w - t)$ and its temporal evolution. Figure 4 shows the recharge date distribution sampled at three different dates : (a) at $t_w^1 = 1994$ under ambient flow conditions, (b) at $t_w^2 = 1994.1$ approximately one month after the pumping started and (c) at $t_w^3 = 1995$ one year after the pumping started. At later dates ($t_w \geq 1995$), distributions stop to evolve. Therefore, only the distribution at $t_w^3 = 1995$ is displayed.

For $1994 \leq t_w \leq 1995$, the system is strongly transient (Figure 4a and b). The start of pumping induces a modification of the recharge date distribution from a narrow piston-like distribution at ambient conditions (t_w^1) (Figure 4a) to a much broader, more exponential-like, later (Figure 4c). Intermediary distribution shapes occur in the first pumping year (Figure 4b). The broadening of the distribution comes from the shift of status of the sampling zone. Under ambient flow conditions, it is a standard zone within the aquifer broken through by just a few flow lines. The different tracers then lead to very close ages (Figure 3). Under pumping conditions, it becomes the major discharge zone of the aquifer focusing a dense net of flow lines that initially discharged in much larger areas such as wetlands (Figure 2) and apparent ages from the different tracers spread out. For $t_w \geq 1994.1$, the recharge date distribution broadens including both shorter and larger residence times than the ambient distribution. In the case of the Plœmeur site, shorter residence times eventually control the apparent ages. This is also consistent with the increase of the mean effective recharge rate and the induced circulation speed up (from 160 mm/year in ambient conditions to 200mm/year in pumping conditions). As previously noted, the distributions sampled in 1995 and later are almost identical. Thus, for $t_w \geq 1995$, sampled concentrations are likely to be more influenced by the temporal evolution of the tracer atmospheric concentrations $C_{in}(t)$ and less by the evolution of the recharge date distribution.

3.2. Effect of the temporal evolution of the recharge date distribution

3.2.1. Methodology

To assess the role of the temporal evolution of the recharge date distribution ($p(t_w - t)$ in equation 12), we filter out the evolution of the tracer atmospheric concentration ($C_{in}(t)$ in equation 12). To this end, we translate the distributions $p_i(t_w^i - t)$ (Table 2) to the same sampling date t_w^t, the exponent "*t*" standing for translated. The recharge date distributions $p_i(t_w^i - t)$ are shifted along the date axis by a translation of $t_w^t - t_w^i$ without any modification of their shape. The shifted distributions are noted $p_i(t_w^t - t)$:

$$p_i(t_w^t - t) = p_i\left(\underbrace{t_w^i - t}_{recharge\ time} + \underbrace{t_w^t - t_w^i}_{translation}\right). \quad (13)$$

This is illustrated on Figure 5 for the three recharge date distributions of Figure 4 translated to $t_w^t = 2009$. The apparent age determination is modified accordingly:

$$A(t_w^t) = t_w^t - C_{in}^{-1}\left(\int_{-\infty}^{t_w^t} C_{in}(t)p_i(t_w^t - t)dt\right). \quad (14)$$

Equation 14 replaces equation 12 and filters out most of the effect of the tracer atmospheric concentration $C_{in}(t)$ to highlight that of the evolution of the flow pattern. The apparent ages

295 are noted $A(t_w^t)$ recalling that they are obtained after the translation of the recharge date
296 distributions.

297 *3.2.2. Results*

298 Figure 6 compares the apparent ages obtained with the various recharge date distributions
299 translated to the same sampling date $t_w^6 = 2009$ for the model numbered 1. The apparent ages
300 are derived from equation 14 and are noted $A(t_w^6)$. As for the apparent ages from equation 12,
301 the apparent ages $A(t_w^t)$ from equation 14 are first almost identical for the four tracers
302 because of the piston-like shape of the ambient distribution. Because of the broadening of the
303 recharge date distributions after the start of pumping, they diverge from each other to finally
304 reach fixed values spreading over almost 15 years (four last points of Figure 6). The apparent
305 ages $A(t_w^t)$ from the distribution initially sampled at $t_w^i = 1994.1$ (*i.e.* one month after the
306 pumping started) constitute an intermediate case. Indeed, unlike the ages from the ambient
307 distribution, they significantly diverge for the four tracers. However, their spreading is not as
308 broad as for the distributions sampled at later dates ($t_w^i \geq 1995$). We will discuss in section
309 4.1 the interest of these differences for model segregation. We have checked that the
310 conclusions were the same for the other sampling dates of Table 2.

311 ## 3.3. Effect of the temporal evolution of the atmospheric
312 concentration

313 *3.3.1. Methodology*

314 To assess the influence of the tracer atmospheric concentration $C_{in}(t)$ independently of the
315 flow pattern modifications, we compute the apparent ages at six translated sampling dates t_w^t
316 (Table 2) for a fixed recharge date distribution. Figure 7 illustrates this analysis for the pseudo
317 transient distribution initially sampled at $t_w^3 = 1995$ and translated to 2004 and 2009. This
318 transformation should not be confounded with the previous one in which we studied the
319 influence of the recharge date distributions at fixed atmospheric concentration $C_{in}(t)$.

320 *3.3.2. Results*

321 Figure 8a, b and c display the results for the three distributions of Figure 4a, b and c. For the
322 ambient distribution (initially arising at $t_w^i = t_w^1 = 1994$), the evolution of $A(t_w^t)$ with t_w^t
323 remains very small (Figure 8a) because of the restricted dispersion of the recharge date
324 distribution (blue curve of Figure 4a). It would be strictly equal to zero for a pure piston-flow
325 model. For broader recharge date distributions corresponding to the pseudo transient case
326 sampled at $t_w^i = t_w^3 = 1995$ (Figure 8c), the apparent ages strongly evolve with t_w^t. The
327 weighting of the recharge date distribution progressively evolves with date and yields
328 different ages consistently with Figure 3. Similar results have been found for the pseudo
329 transient distributions sampled after t_w^3 (≥1995). For the distribution initially sampled one
330 month after the pumping started (at $t_w^i = 1994.1$), the apparent age variation with t_w^t is still
331 significant though less important than the age variation from the posterior distributions.

In conclusion, the two previous analyses highlight the respective effects of the recharge date distribution (3.2) and of the tracer atmospheric concentration (3.3). They show two well-differentiated regimes of apparent age evolution. The first regime occurs within the first few months after starting the pumping. Note that it is fast in comparison to the mean residence time (50 years). The recharge date distribution shifts from a restricted distribution to an extended one with major consequences on apparent ages. Relatively parallel flow lines under ambient conditions become convergent under pumping inducing the broadening of the recharge date distribution. By comparison, on these short durations (some months), the evolution of the atmospheric concentration has a negligible effect. The second regime occurs after the first year of pumping and lasts for longer period of times. The recharge date distribution marginally changes without any marked effect on the apparent ages. The dominant source of age variation is the non-linear evolution of the tracer atmospheric concentration. This reveals that apparent ages can significantly evolve even if fluid flows and transport are at steady-state. If the second regime is smoother than the first one, it still leads to significant variation of ages (Figure 3).

4. Discussion

We first discuss the potential interest of the two successive evolutions of apparent ages, *i.e.* a first phase dominated by the transient flow pattern and a second one by the transient atmospheric concentration for flow pattern characterization and models segregation. We secondly compare these modeling results to the available data on the site of Plœmeur.

4.1. Information contained in the temporal evolution of apparent ages

The temporal evolution of apparent ages contains information on the hydrogeological system, in addition to information contained in the tracer concentrations analyzed at a single time. Yet, information is largely different between the two evolutions identified in sections 3.2 and 3.3. The first evolution is the rapid shift when starting pumping from a restricted recharge date distribution to an extended one. The restricted recharge date distribution can be typically fitted by an inverse Gaussian model characterizing mainly the length of the flow paths from the recharge zone divided by the recharge rate (Ginn et al., 2009; Woolfenden and Ginn, 2009). The broader recharge date distribution characterizes more globally the aquifer volume and the overall recharge rate (Leray et al., 2012), so does typically the exponential model (Haitjema, 1995). Therefore, almost independent and useful pieces of information, such as a characteristic length *vs.* a volume, can be obtained using the same well before and after the start of pumping. Using equation 12 as an illustration, it comes down to use the temporal evolution of apparent ages to estimate the transient controlling parameters of the function $p(t_w - t)$.

Figure 9 compares the temporal evolution of the CFC-12 age for the models numbered 1 and numbered 2 (Table 1) at sampling dates ranging from 1994 to 2009 (Table 2). It shows that the two models give distinct apparent ages before 1995 *i.e.* when the recharge date distribution is transient. Later, once the recharge date distribution is broad and reaches a steady-state, and because the two models have been calibrated on CFC-12 age in 2009, the apparent ages are identical for both models. Differences only occur at short term after the pumping started and result from different transient evolutions of the residence time distribution. This underlines the interest of a continuous sampling of environmental tracer concentrations, particularly at the early times of pumping, to characterize the transient behavior of the system. In that case, apparent age time series can be used as an additional tool

to segregate hydrogeological models. Using equation 12 as an illustration, it comes down to use the temporal signal in apparent ages to segregate two functions $p(t_w - t)$ that exhibit distinct transient behaviors.

4.2. Comparison to field observations on the site of Plœmeur

Apparent ages obtained from CFC-11, CFC-12, CFC-113 and SF_6 data have been determined on the site of Plœmeur since 2006 and recorded in the Plœmeur site database (Ayraud et al., 2008; de Dreuzy et al., 2006). In the pumping well, data are available in 2006 and 2009. CFC-12 age increases from 27.5 in 2006 to 30 years in 2009 and CFC-113 age decreases from 28.5 to 26.5 years. CFC-11 ages are close to 45 years and remain constant with time. Still, they should be very close to CFC-12 apparent ages because of the similar normalized atmospheric concentrations of the two tracers. As already reported in Leray et al. (2012), degradation of CFC-11 under anaerobic conditions may explain these differences (Cook and Solomon, 1995). SF_6 apparent ages are less than 10 years. Such discrepancies cannot be explained by hydrodynamic mixing alone even at the pumping well (Leray et al., 2012) but are rather coming some geogenic production from the neighboring granites (Busenberg and Plummer, 2000; Koh et al., 2007).

The results of the models in section 3 suggest that with negligible temporal change of the recharge date distribution, the apparent age should continuously increase whatever the tracer and within the date interval 2000-2010. The CFC-12 age increase at the Plœmeur site is similar in terms of magnitude to that of the models. CFC-12 data thus suggest that the tracer age evolution in that discharge area mainly comes from the temporal evolution of the atmospheric concentration weighting and that the flow pattern and the resulting recharge date distribution in the pumping zone are in turn not expected to vary significantly after 2006.

Still, CFC-113 exhibits an opposite age variation in comparison with CFC-12. Considering the age uncertainty due to analytical and sampling errors (Leray et al., 2012), the acquisition of additional concentration data over the next few years would help to confirm the age trends and eventually conclude about the flow pattern stabilization.

Earlier flow conditions, and particularly initial ones *i.e.* just before the pumping started, are more difficult to constrain on the site of Plœmeur because of the lack of environmental tracers monitoring before 2006. Contrary to CFCs and SF_6 data, chloride and nitrate concentrations have been monitored on a longer date range starting at 1991. Because of reactivity processes and their evolution with time, the nitrate concentration chronicle can only give partial information on the flow pattern and on mixing processes. However, its non-negligible initial concentration (roughly 15 mg/l) before the start of pumping indicates short residence times consistent with the local recharge area and the short flow paths obtained in the models. Chloride has the advantage of being conservative and being characteristic of deeper waters and thus a good indicator of the flow pattern and its evolution. Figure 10 represents the temporal evolution of chloride concentration at the pumping well. It displays a sharp increase during the first two years of pumping (1^{st} phase of Figure 10), a very slight increase for the next ten years (2^{nd} phase of Figure 10) and finally stabilizes after 2005 (3^{rd} phase of Figure 10). The first phase is consistent with the previous modeling result of a quick transition from the piston-like recharge date distribution to the more extended one. The short duration of the first phase is consistent with the fast temporal evolution of the recharge area (Figure 11). Before pumping, the recharge area is a small zone upstream of the well (blue line). It quickly expands to a much larger area around the well only after one year of pumping (green line). Actually, the pumping well collects water that naturally discharged in wetlands next to it and transforms a wide discharge zone to a point-like one.

The 2nd phase corresponds to a slight increase of the chloride concentration (Figure 10). This increase does not come from the changes of the recharge area induced by the evolution of the flow pattern, in this case marginal (from orange to purple curves in Figure 11). It more likely comes from the modification of the deep water fraction coming from the main aquifer - *i.e.* the contact zone - that dips quasi-vertically at about 1,500m from the pumping well (Figure 11, (Ruelleu et al., 2010)). Its evolution only affects recharge dates earlier than 1940 and cannot consequently be detected by atmospheric gases. Finally, the stabilization of the chloride concentration (3rd phase of Figure 10) agrees with the apparition of a new steady-state regime.

5. Conclusion

We have analyzed the temporal evolution of apparent ages in a complex aquifer under pumping based on CFCs and SF_6 concentrations measured at the pumping well. The evolution of apparent ages at the pumping well with time can come from (1) the transient nature of flow conditions and (2) the transient evolution of the tracer atmospheric concentrations. To identify the respective role of these two sources, we proposed two successive analyses of the residence time distributions: (1) convolution at the same sampling date (*i.e.* with the same atmospheric concentration chronicle) of residence time distributions initially arising at different dates to assess the effect of the distributions, (2) convolution of one residence time distribution at various sampling dates (*i.e.* with various atmospheric concentration chronicles) to assess the effect of the atmospheric concentration.

We identify two well-differentiated phases in the evolution of apparent ages. Apparent ages first evolve because of the pumping-induced modifications of flows. At this stage, the temporal evolution of apparent ages is distinct between two hydrogeological models and may

448 be advantageously used to segregate them using for instance a classical least square
449 comparison procedure of data with modeling results. The transient measure of the tracer
450 concentrations contain some additional information and slightly compensate for the small
451 number of available tracers. After one year of pumping, residence time distributions hardly
452 evolve and apparent ages become solely modified by the transient evolution of the
453 atmospheric concentrations. Apparent ages still significantly evolve but do not contain any
454 additional information on the flow patterns beyond those contained in the steady-state data.

455 ## Acknowledgments

456 Funding was provided by the French National Research Agency ANR through the H2MNO4
457 project for the development of parallel simulation methods (ANR-11-MN). Research and
458 monitoring on the site of Plœmeur is funded by the Environmental research Observatory H+
459 (Network of hydrogeological sites) and by the European Interreg IV project Climawat. J.-R.
460 de Dreuzy acknowledges the European Union for its additional funding through the IEF
461 Marie-Curie fellowship (PIEF-GA-2009-251710). The authors acknowledge Arash
462 Massoudieh and an anonymous reviewer for their fruitful reviews.

463

464

References

Ayraud, V., 2005. Détermination du temps de résidence des eaux souterraines: application au transfert d'azote dans les aquifères fracturés hétérogènes. Ph.D Thesis, Université de Rennes 1, Rennes, 312 pp.

Ayraud, V., Aquilina, L., Labasque, T., Pauwels, H., Molenat, J., Pierson-Wickmann, A.-C., Durand, V., Bour, O., Tarits, C., Le Corre, P., Fourre, E., Merot, P., Davy, P., 2008. Compartmentalization of physical and chemical properties in hard-rock aquifers deduced from chemical and groundwater age analyses. Applied geochemistry, 23(9): 2686-2707. doi:10.1016/j.apgeochem.2008.06.001.

Bear, J., 1991. Modelling and applications of transport phenomena in porous media. Theory and applications of transport in porous media. Kluwer Academic Publishers, Dordrecht.

Bredehoeft, J.D., 2002. The Water Budget Myth Revisited: Why Hydrologists Model. Groundwater, 40(4): 340-345.

Bresciani, E., Davy, P., de Dreuzy, J.-R., 2011. A finite volume approach with local adaptation scheme for the simulation of free surface flow in porous media. International Journal For Numerical and Analytical Methods in Geomechanics, 36(13): 1574-1591. doi:10.1002/nag.1065.

Busenberg, E., Plummer, L.N., 2000. Dating young groundwater with sulfur hexafluoride: Natural and anthropogenic sources of sulfur hexafluoride. Water Resour. Res., 36(10): 3011-3030. doi:10.1029/2000WR900151.

Carn, A., 1990. Mise en valeur des ressources en eau souterraine du socle breton.Département du Morbihan (35) - R31724 BRE 4S/90, BRGM, Rennes.

Castro, M.C., Goblet, P., Ledoux, E., Violette, S., de Marsily, G., 1998. Noble gases as natural tracers of water circulation in the Paris Basin, 2. Calibration of a groundwater flow model using noble gas isotope data. Water Resour. Res., 34(10): 2467-2483.

Cook, P.G., Love, A.J., Robinson, N.I., Simmons, C.T., 2005. Groundwater ages in fractured rock aquifers. Journal of Hydrology, 308(1-4): 284-301. doi:10.1016/j.jhydrol.2004.11.005.

Cook, P.G., Solomon, D.K., 1995. Transport of atmospheric trace gases to the water table - Implications for groundwater dating with chlorofluorocarbons and krypton-85. Water Resour. Res., 31(2): 263-270. doi:10.1029/94WR02232.

de Dreuzy, J.-R., Beaudoin, A., Erhel, J., 2007. Asymptotic dispersion in 2D heterogeneous porous media determined by parallel numerical simulations Water Resour. Res., 43(10). doi:10.1029/2006WR005394.

de Dreuzy, J.-R., Bodin, J., Le Grand, H., Davy, P., Boulanger, D., Battais, A., Bour, O., Gouze, P., Porel, G., 2006. General database for ground water site information. Groundwater, 44(5): 743-748. doi:0.1111/j.1745-6584.2006.00220.x.

de Marsily, G., 1986. Quantitative hydrogeology: Groundwater Hydrology for Engineers. Academic Press, New-York, 440 pp.

505 Erhel, J., de Dreuzy, J.-R., Bresciani, E., 2008. Multi-parametric intensive stochastic
506 simulations for hydrogeology on a computational grid. In: Tromeur-Dervout, D.,
507 Brenner, G., Emerson, D., Erhel, J. (Eds.), Parallel Computational Fluid Dynamics.
508 Springer, Lecture Notes in Computational Science and Engineering, pp. 389-397.

509 Erhel, J., de Dreuzy, J.R., Beaudoin, A., Bresciani, E., Tromeur-Dervout, D., 2009. A parallel
510 scientific software for heterogeneous hydrogeoloy. In: Tuncer, I.H., Gulcat, U.,
511 Emerson, D.R., Matsuno, K. (Eds.), Parallel Computational Fluid Dynamics 2007.
512 Lecture Notes in Computational Science and Engineering. Springer, pp. 39-48.

513 Frind, E.O., Muhammad, D.S., Molson, J.W., 2005. Delineation of Three-Diemnsional Well
514 Capture Zones for Complex Multi-Aquifer Systems. Groundwater, 40(6).
515 doi:10.1111/j.1745-6584.2002.tb02545.x.

516 Ginn, T.R., Haeri, H., Massoudieh, A., Foglia, L., 2009. Notes on Groundwater Age in
517 Forward and Inverse Modeling. Transport in Porous Media, 79(1): 117-134.
518 doi:10.1007/s11242-009-9406-1.

519 Haitjema, H.M., 1995. On the residence time distribution in idealized groundwatesheds. J.
520 Hydrol., 172(1-4): 127-146. doi:10.1016/0022-1694(95)02732-5.

521 IAEA, 2006. Use of chlorofluorocarbons in hydrology : a guidebook. International Atomic
522 Energy Agency, Vienna, 277 pp.

523 Kinzelbach, W., 1988. The random-walk method in pollutant transport simulation. In:
524 Custodio, E., Gurgui, A., Lobo Ferreira, J.P. (Eds.), Groundwater flow and quality
525 modelling. NATO ASI. Dordrecht, New York, pp. 227-246.

526 Koh, D.-C., Plummer, L.N., Busenberg, E., Kim, Y.-J., 2007. Evidence for terrigenic SF_6 in
527 groundwater from basaltic aquifers, Jeju Island, Korea : Implications for groundwater
528 dating. J. Hydrol., 339(1-2): 93-104. doi:10.1016/j.jhydrol.2007.03.011.

529 Kreft, A., Zuber, A., 1978. On the physical meaning of the dispersion equation and its
530 solution for different initial and boundary conditions. Chemical Engineering Science,
531 33(11): 1471-1480. doi:10.1016/0009-2509(78)85196-3.

532 LaBolle, E.M., Fogg, G.E., 2001. Role of molecular diffusion in contaminant migration and
533 recovery in an alluvial aquifer system. Transp. Porous Media, 42(1-2): 155-179.
534 doi:10.1023/A:1006772716244.

535 Le Borgne, T., Bour, O., de Dreuzy, J.-R., Davy, P., Touchard, F., 2004. Equivalent mean
536 flow models for fractured aquifers: Insights from a pumping tests scaling
537 interpretation. Water Resour. Res., 40(3). doi:10.1029/2003WR002436.

538 Le Borgne, T., Bour, O., Paillet, J.-L., Caudal, J.-P., 2006. Assessment of preferential flow
539 path connectivity, and hydraulic properties at single-borehole and cross-borehole
540 scales in a fractured aquifer. J. Hydrol., 328(1-2): 347-359.

541 Leray, S., de Dreuzy, J.R., Bour, O., Bresciani, E., 2013. Numerical modeling of the
542 productivity of vertical to shallowly dipping fractured zones in crystalline rocks. J.
543 Hydrol., 481: 64-75.

544 Leray, S., de Dreuzy, J.R., Bour, O., Labasque, T., Aquilina, L., 2012. Contribution of age
545 data to the characterization of complex aquifers. J. Hydrol., 464-465: 54-68.
546 doi:10.1016/j.jhydrol.2012.06.052.

Long, A.J., Putnam, L.D., 2009. Age-distribution estimation for karst groundwater : Issues of parameterization and complexity in inverse modeling by convolution. J. Hydrol., 376: 579-588.

Maloszewski, P., Zuber, A., 1982. Determining the turnover time of groundwater systems with the aid of environmental tracers, 1. Models and their applicability. J. Hydrol., 57(3-4): 207-231.

McMahon, P.B., Carney, C.P., Poeter, E.P., Peterson, S.M., 2010. Use of geochemical, isotopic, and age tracer data to develop models of groundwater flow for the purpose of water management, northern High Plains aquifer, USA. Applied geochemistry, 25: 910-922. doi:10.1016/j.apgeochem.20120.04.001.

Neupauer, R.M., Wilson, J.L., 1999. Adjoint method for obtaining backward-in-time location and travel time probabilities of a conservative groundwater contaminant. Water Resour. Res., 35(11): 3389–3398. doi:10.1029/1999WR900190.

Neupauer, R.M., Wilson, J.L., 2001. Adjoint-derived location and travel time probabilities for a multidimensional groundwater system. Water Resour. Res., 37(6): 1657-1668. doi:10.1029/2000WR900388.

Neupauer, R.M., Wilson, J.L., 2002. Backward probabilistic model of groundwater contamination in non-uniform and transient flow. Advances in Water Resources, 25(7): 733-746.

Nir, A., 1964. On the interpretation of tritium 'Age' measurements of groundwater. journal of Geophysical Research, 69(1): 2589-2595.

Ruelleu, S., Moreau, F., Bour, O., Gapais, D., Martelet, G., 2010. Impact of gently dipping discontinuities on basement aquifer recharge: An example from Plœmeur (Brittany, France). Journal of Applied Geophysics, 70(2): 161-168. doi:10.1016/j.jappgeo.2009.12.007.

Sanford, W.E., Plummer, L.N., McAda, D.P., Bexfield, L.M., Anderholm, S.K., 2004. Hydrochemical tracers in the middle Rio Grande Basin, USA: 2. Calibration of a groundwater-flow model. Hydrogeol. J., 12(4): 389-407. doi:10.1007/s10040-004-0326-4.

Schwartz, F.W., Sudicky, E.A., McLaren, R.G., Park, Y.-J., Huber, M., Apted, M., 2010. Ambiguous hydraulic heads and ^{14}C activities in transient regional flow. Groundwater, 48(3): 366-379.

Sophocleous, M., 2005. Groundwater recharge and sustainibility in the high Plains aquifer in Kansas, USA. Hydrogeol. J., 13: 351-365. doi:10.1007/s10040-004-0385-6.

Stichler, W., Maloszewski, P., Bertleff, B., Watzel, R., 2008. Use of environmental isotopes to define the capture zone of a drinking water supply situated near a dredge lake. J. Hydrol., 362: 220-233. doi:10.1016/j.jhydrol.2008.08.024.

Touchard, F., 1999. Caractérisation hydrogéologique d'un aquifère en socle fracturé : Site de Plœmeur (Morbihan). PhD Thesis, University of Rennes 1, France, 343 pp.

Troldborg, L., Jensen, K.H., Engesgaard, P., Refsgaard, J.C., Hinsby, K., 2008. Using environmental tracers in modeling flow in a complex shallow aquifer system. J. Hydrol. Eng., 13(11): 1037-1048. doi:10.1061/(asce)1084-0699(2008)13:11(1037).

589 Waugh, D.W., Hall, T.M., Haine, T.W.N., 2003. Relationships among tracer ages. Journal of
590 Geophysical Research, 108(C5): 3138. doi:10.1029/2002JC001325.

591 Woolfenden, L.R., Ginn, T.R., 2009. Modeled ground water age distributions. Groundwater,
592 47(4): 547-557.

593 Zhang, Y., 2004. Numerical simulations of dating young groundwater with multiple
594 atmospheric tracers : CFC-11, CFC-12, SF_6, $^{3}H/^{3}He$ and ^{85}Kr. In: Miller, C.T.,
595 Farthing, M.W., Gray, W.G., Pinder, G.F. (Eds.), 15th International Conference on
596 Computational Methods in Water Resources. Developments in Water Science.
597 Elsevier Science BV, Chapel Hill, NC, pp. 1367-1378.

598 Zinn, B.A., Konikow, L.F., 2007. Potential effects of regional pumpage on groundwater age
599 distribution. Water Resour. Res., 43(6). doi:10.1029/2006WR004865.

600 Zuber, A., Rozanski, K., Kania, J., Purtschert, R., 2011. On some methodological problems in
601 the use of environmental tracers to estimate hydrogeologic parameters and to calibrate
602 flow and transport models. Hydrogeol. J., 19: 53-69.

603

604

Tables

Table 1: Parameters of the two hydrogeological models of the site of Plœmeur used in this study with their reference work. H_{TOT} represents the mean thickness of the aquifer system composed of the micaschists and of the contact zone (Figure 1). The two models have been calibrated on the piezometric level at the pumping well and on CFC-12 apparent age at the pumping well.

Table 2 : Sampling dates t_w^i where the apparent ages are determined.

Figures

Figure 1: 3D diagram of the hydrogeological conceptual model composed of the contact zone, the North 20° normal fault, the micaschists and the two granites. The North 20° normal fault is underlined by black stripes. The red triangle locates the sampled pumping well. $H(x)$ represents the thickness of the aquifer system composed of the micaschists and the contact zone. Its mean, noted H_{TOT}, is taken as a proxy for the characterization of its structure. As a convention, all positions are given in meters and vertical positions are negative below the sea level and positive above. Adapted from Leray et al. (2012).

Figure 2: Boundary conditions applied to the model *i.e.* no flow on the East and the West boundaries (black lines) and head imposed on the North and South boundaries (red lines). The limits with the impervious granites are represented by black dashed lines. Discharge zones in ambient conditions (green) are partly dried with starting the pumping. Specifically, the wetland in the pumping zone entirely disappears. Figure 3: Apparent ages derived from CFCs and SF_6 concentrations as functions of the sampling date t_w for the model numbered 1 (Table 1).

Figure 4: Recharge date distributions $p(t_w - t)$ of the model numbered 1 (solid curves, left axis) superimposed on CFC-12 atmospheric concentration $C_{in}(t)$ (grey dashed line, right axis). Recharge date distributions are sampled at: a) t_w^1 (1994 – ambient flow, blue curve), b) t_w^2 (1994.1, wine curve), and c) t_w^3 (1995, green curve). Superposition of the curves shows the sampling of the tracer atmospheric concentration performed by the recharge date distributions.

Figure 5: CFC-12 atmospheric concentration $C_{in}(t)$ (grey dashes) superimposed on some translated distributions $p_i(t_w^t - t)$ to the sampling date $t_w^t = 2009$ for the model numbered 1 (Table 1). The translated distributions are the ambient distribution (initially sampled at $t_w^1 = 1994$, blue curve) and two pseudo transient distributions initially sampled at $t_w^2 = 1994.1$ (wine curve) and at $t_w^3 = 1995$ (green curve). Note that the ordinate axis has been broken between 0.05 and 0.19 to display the peak of the ambient distribution.

Figure 6: Apparent ages derived from CFCs and SF_6 concentrations for the translated recharge date distributions $p_i(t_w^6 - t)$ with *i* from 1 to 6 for the model numbered 1 (Table 2). p_1 corresponds to the blue curve of the Figure 5 (translated ambient distribution), p_2 to the wine curve of the Figure 5 and p_3 to the green curve of the Figure 5.

Figure 7: Recharge date distribution p_3 at its initial sampling date $t_w^3 = 1995$ (green solid curve) and translated to $t_w^t = 2004$ (green dash dots) and translated to $t_w^t = 2009$ (green short dashes) for the model numbered 1 (left axis) superimposed on the CFC-12 atmospheric concentration $C_{in}(t)$ (grey dashed line, right axis)

Figure 8: Apparent ages derived from CFCs and SF_6 concentrations as functions of the translated sampling date t_w^t for the model numbered 1. Apparent ages are obtained for (a) the translated ambient distribution $p_1(t_w^t - t)$ (blue curve of Figure 4a), (b) the translated

651 pseudo transient distribution $p_2(t_w^t - t)$ (wine curve of Figure 4b) and (c) the translated

652 pseudo transient distribution $p_3(t_w^t - t)$ (green curve of Figure 4c).

653 Figure 9: CFC-12 ages of the model numbered 2 (blue crosses) as a function of CFC-12 ages
654 of the model numbered 1 (Table 1). CFC-12 ages are computed at the pumping well and at
655 sampling dates between 1994 and 2009 (Table 2). Labels next to the crosses stand for the
656 corresponding sampling dates. We recall that the two models have both been calibrated on the
657 CFC-12 age in 2009. Results for the tracers CFC-11, CFC-113 and SF_6 are similar and thus
658 are not shown.

659 Figure 10: Chloride concentration as a function of the sampling date t_w measured at the
660 pumping well of the site of Plœmeur (updated from Ayraud (2005)). The first phase consists
661 in a sharp and fast increase of the chloride concentration, the second phase in a slight increase
662 of the chloride concentration and the third phase in the stabilization of the chloride
663 concentration.

664 Figure 11: Surface origin of the CFCs and SF6 (corresponding to recharge dates posterior to

665 1940) for the model numbered 1 (Table 1) under pseudo transient conditions sampled at t_w^1

666 (1994 – ambient flow, blue line), at t_w^2 (1994.1, wine line), at t_w^3 (1995, green line), at t_w^4

667 (1999, orange line), at t_w^5 (2004, red line) and at t_w^6 (2009, purple wine).

	Values		References
Common parameters			
Potential recharge rate R (mm/year)	200		(Carn, 1990; Touchard, 1999)
Granites conductivity K_G (m/s)	10^{-11}		
Specific parameters for selected models			
	Model n°1	Model n°2	
Mean thickness H_{TOT} (m) – structure name	180 - shallow	280 - deep	(Ruelleu et al., 2010)
Micaschists permeability K_{MS} (m/s)	10^{-6}	$5x10^{-6}$	(Leray et al., 2012)
Contact zone transmissivity T_{CZ} ($x10^{-3}$ m^2/s)	2.27	2.2	(Le Borgne et al., 2004; Le Borgne et al., 2006)
North20° fault transmissivity ($x10^{-3}$ m^2/s)	1.14	1.1	(Le Borgne et al., 2004; Le Borgne et al., 2006)
Porosity φ (%)	5	2.7	(Leray et al., 2012)

Table2

Sampling dates t_w	Acronym	Name and color for corresponding $p\ (t_w - t)$
1994	t_w^1	$p_1 = p\ (t_w^1 - t)$, blue
1994.1	t_w^2	$P_2 = p\ (t_w^2 - t)$, wine
1995	t_w^3	$P_3 = p\ (t_w^3 - t)$, green
1999	t_w^4	$p_4 = p\ (t_w^4 - t)$, not displayed
2004	t_w^5	$p_5 = p\ (t_w^5 - t)$, not displayed
2009	t_w^6	$p_6 = p\ (t_w^6 - t)$, not displayed

Figure1

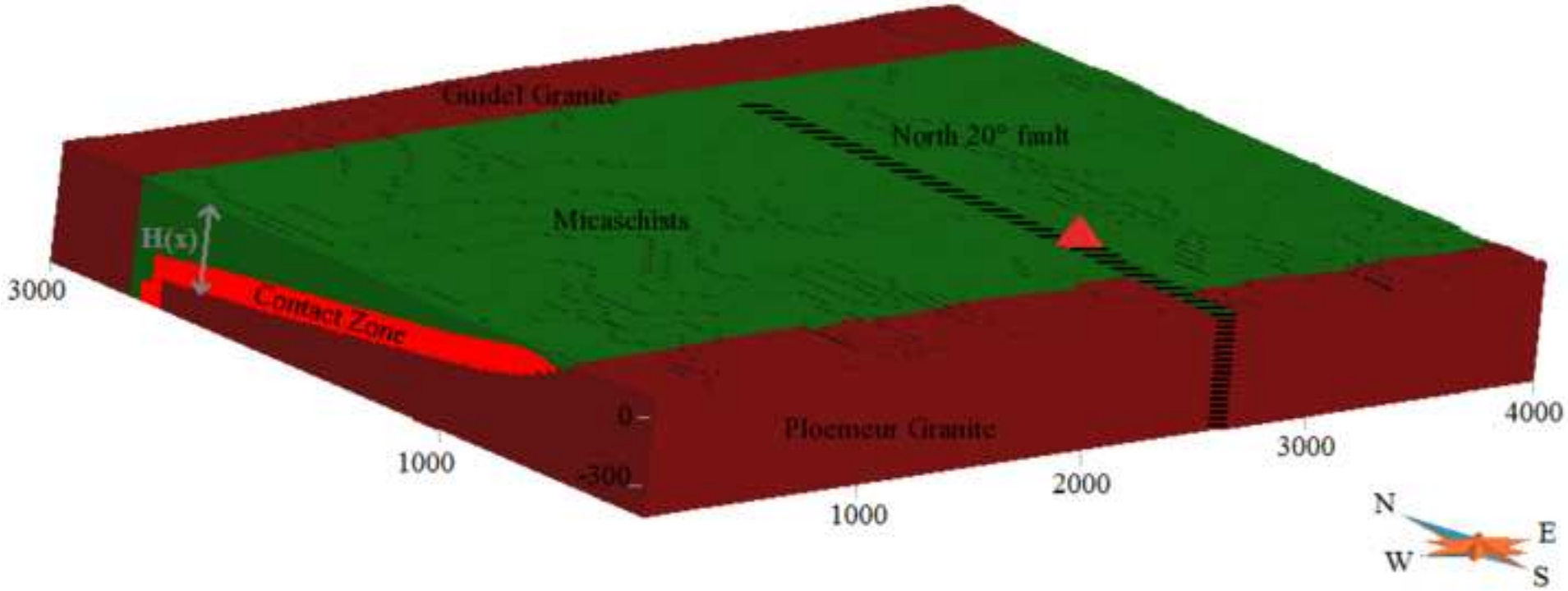

Figure2

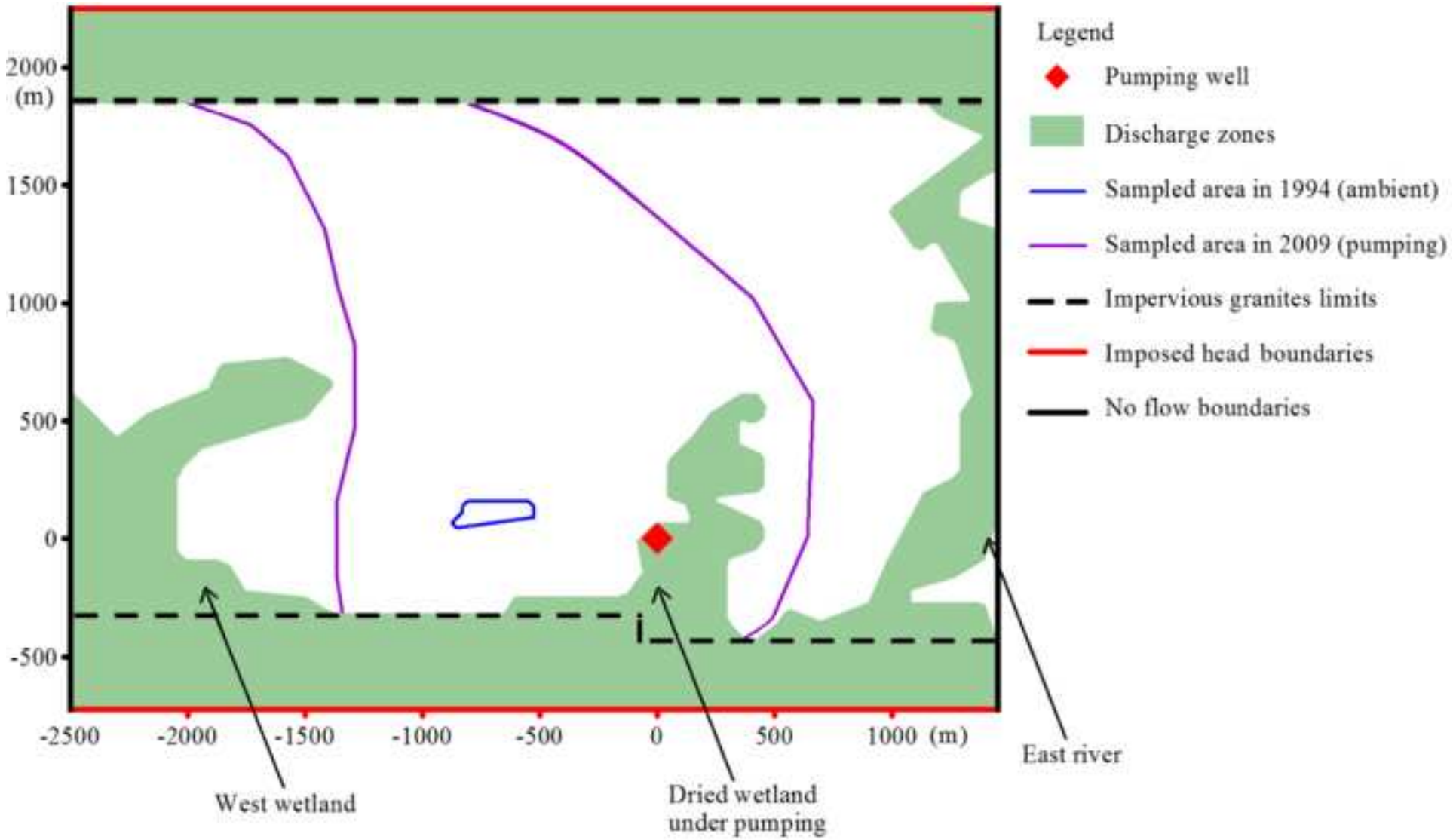

Figure3

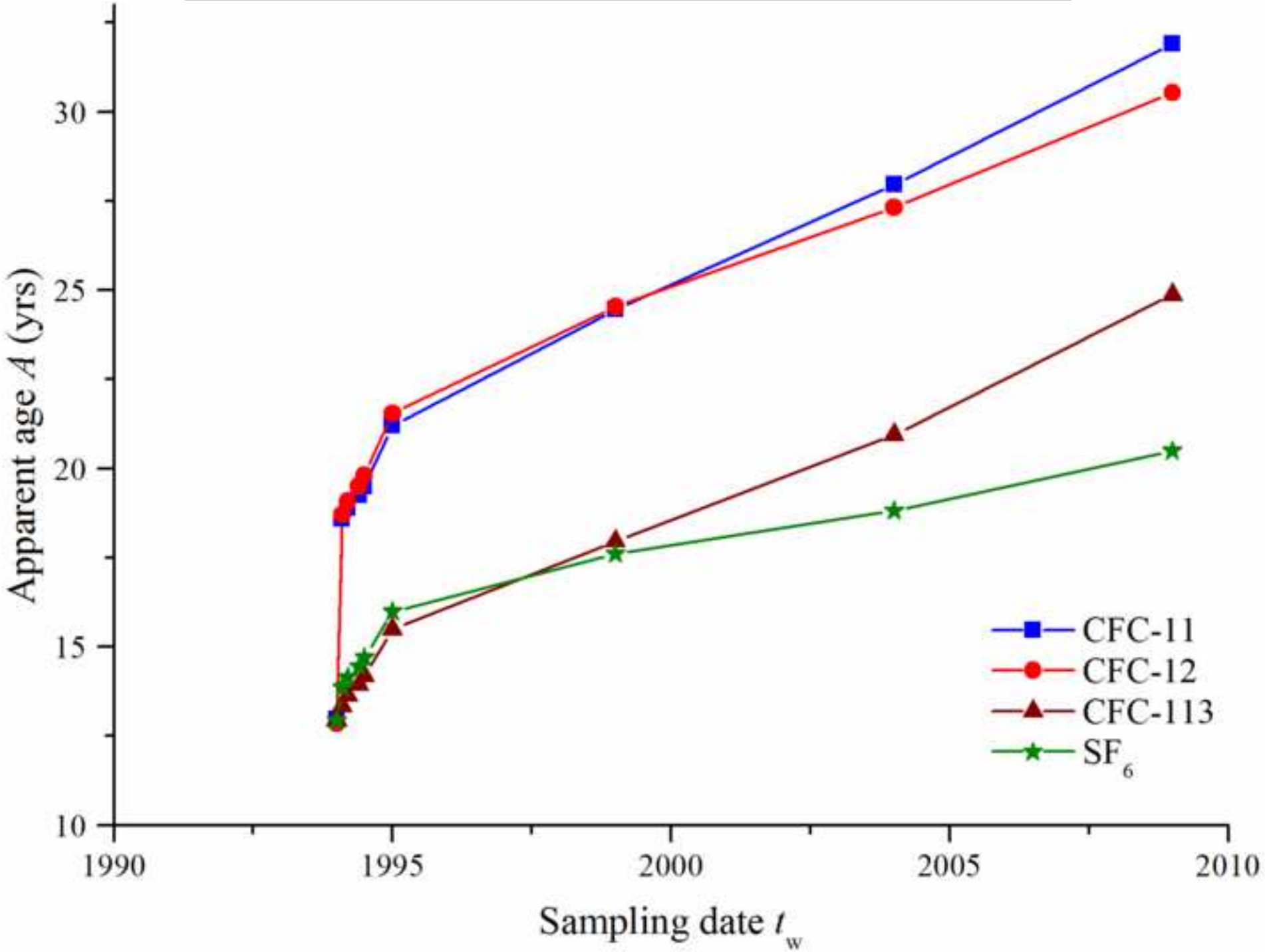

Figure4

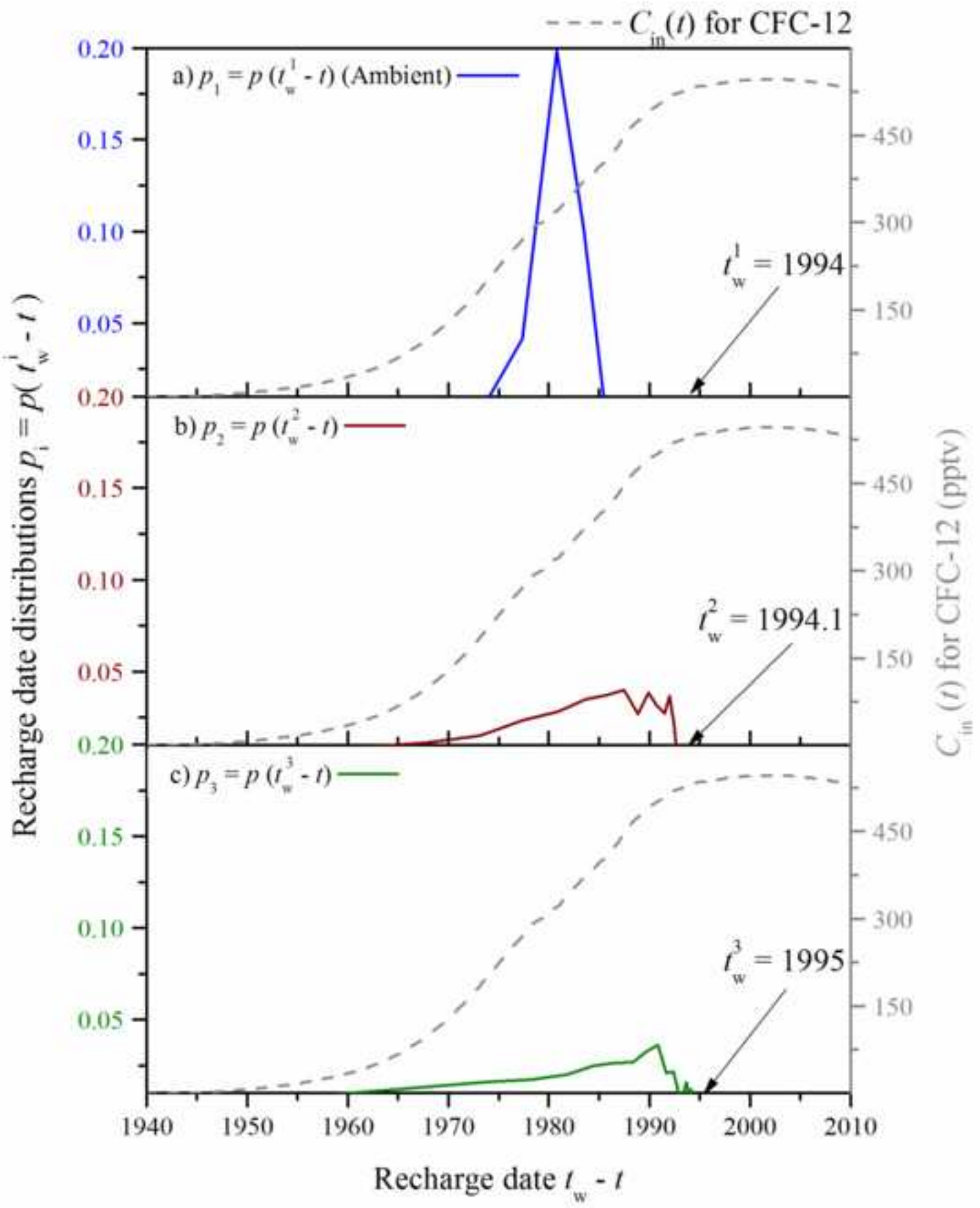

Figure5

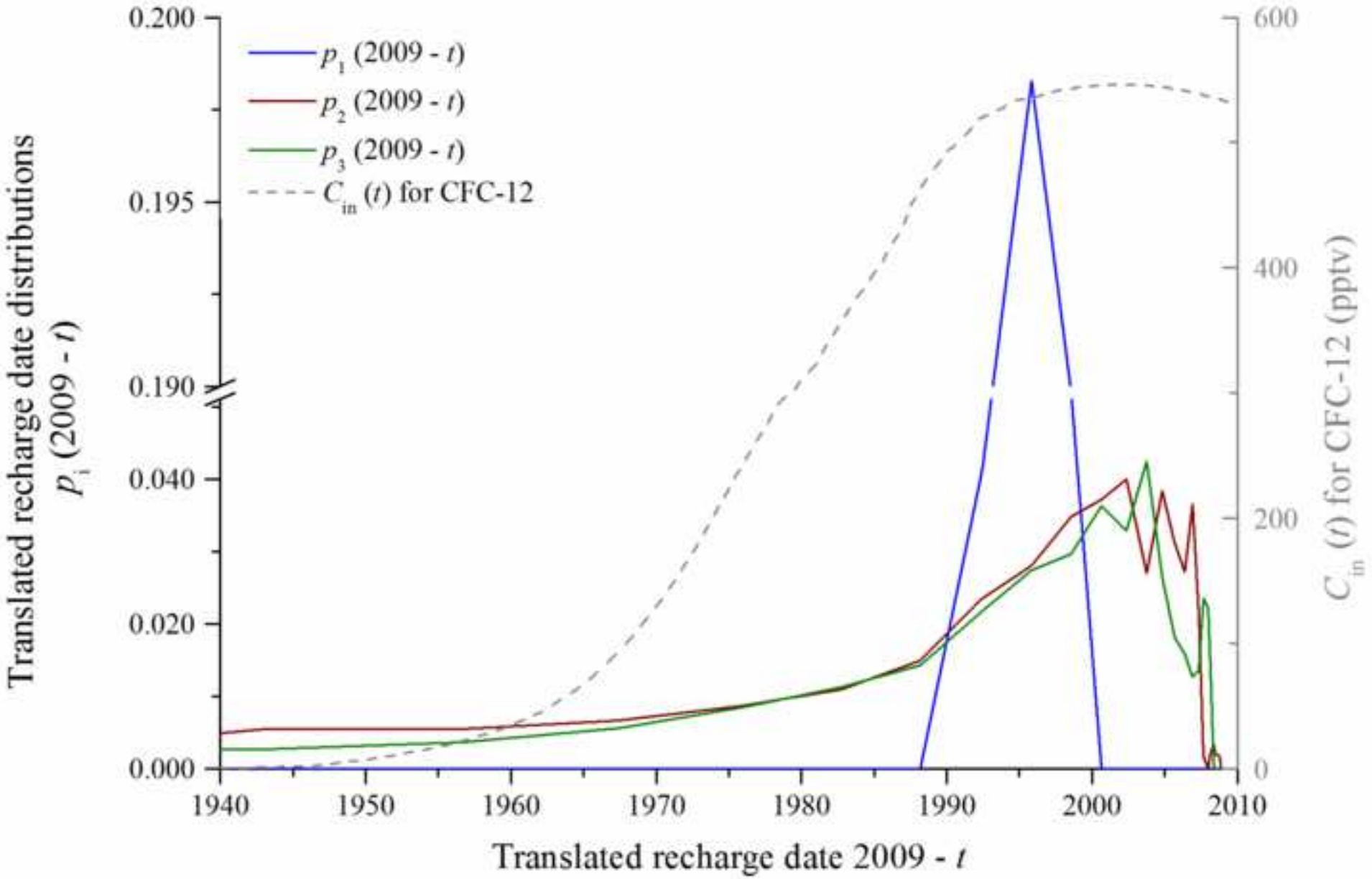

Figure6

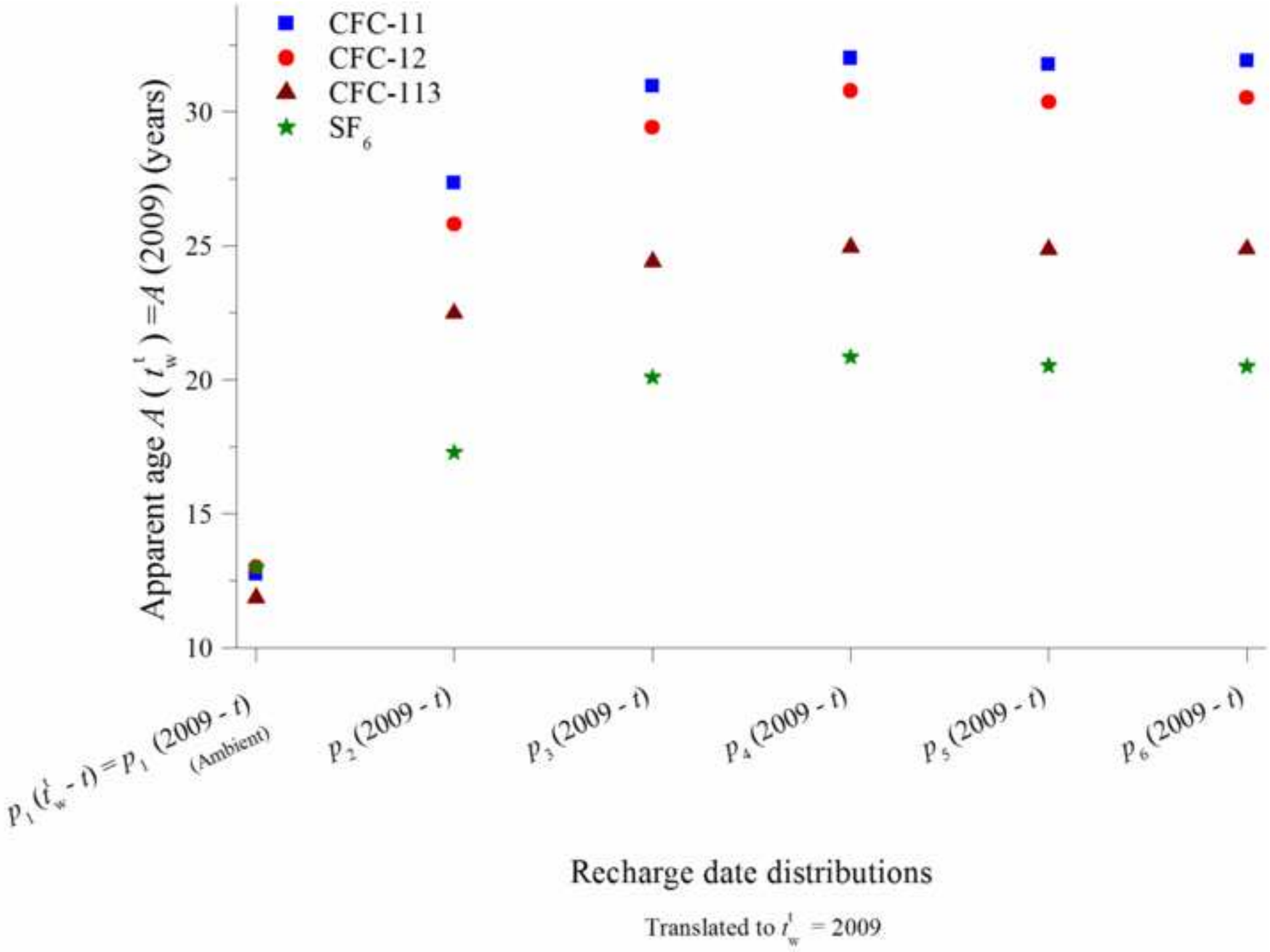

Figure7

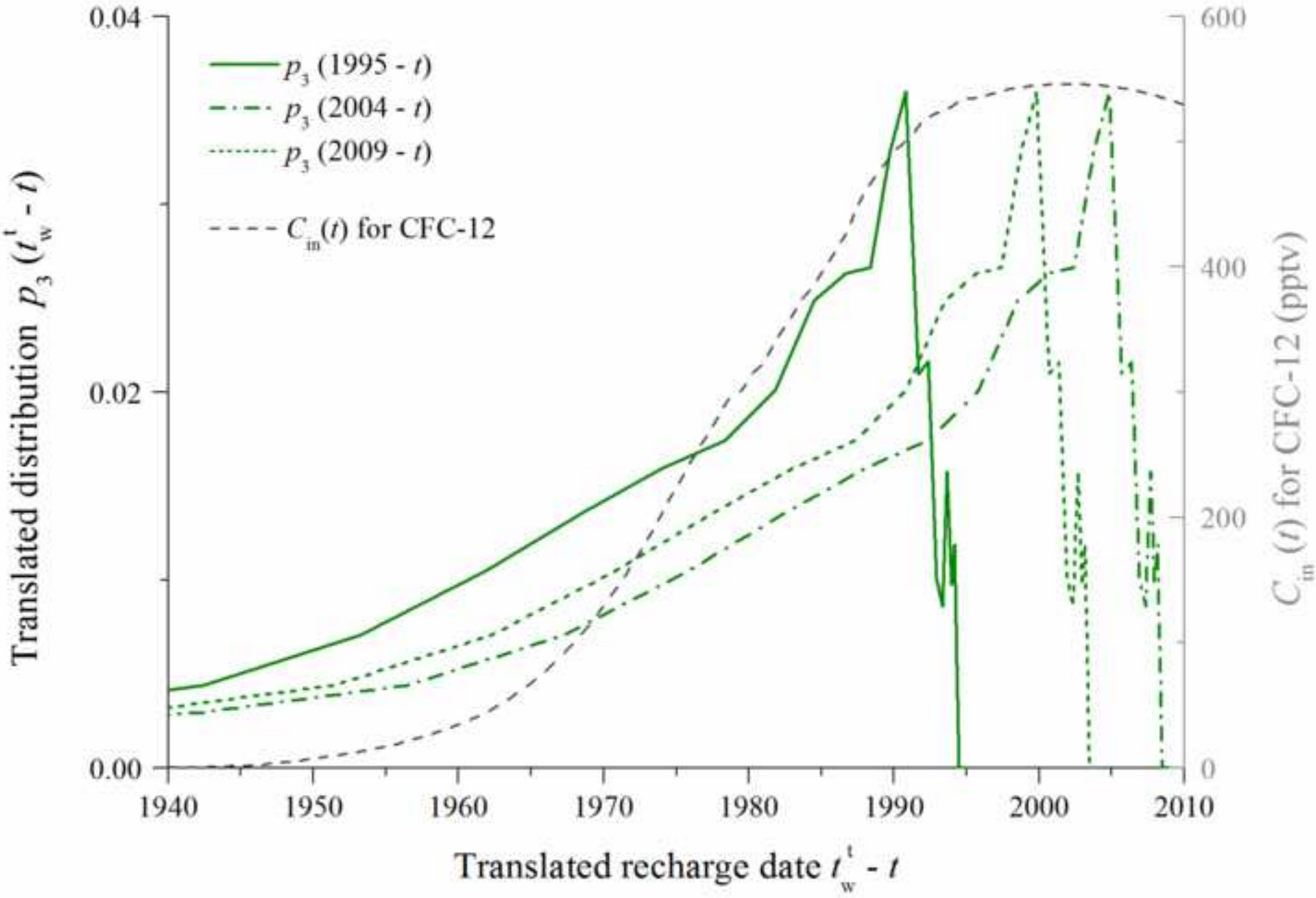

Figure8

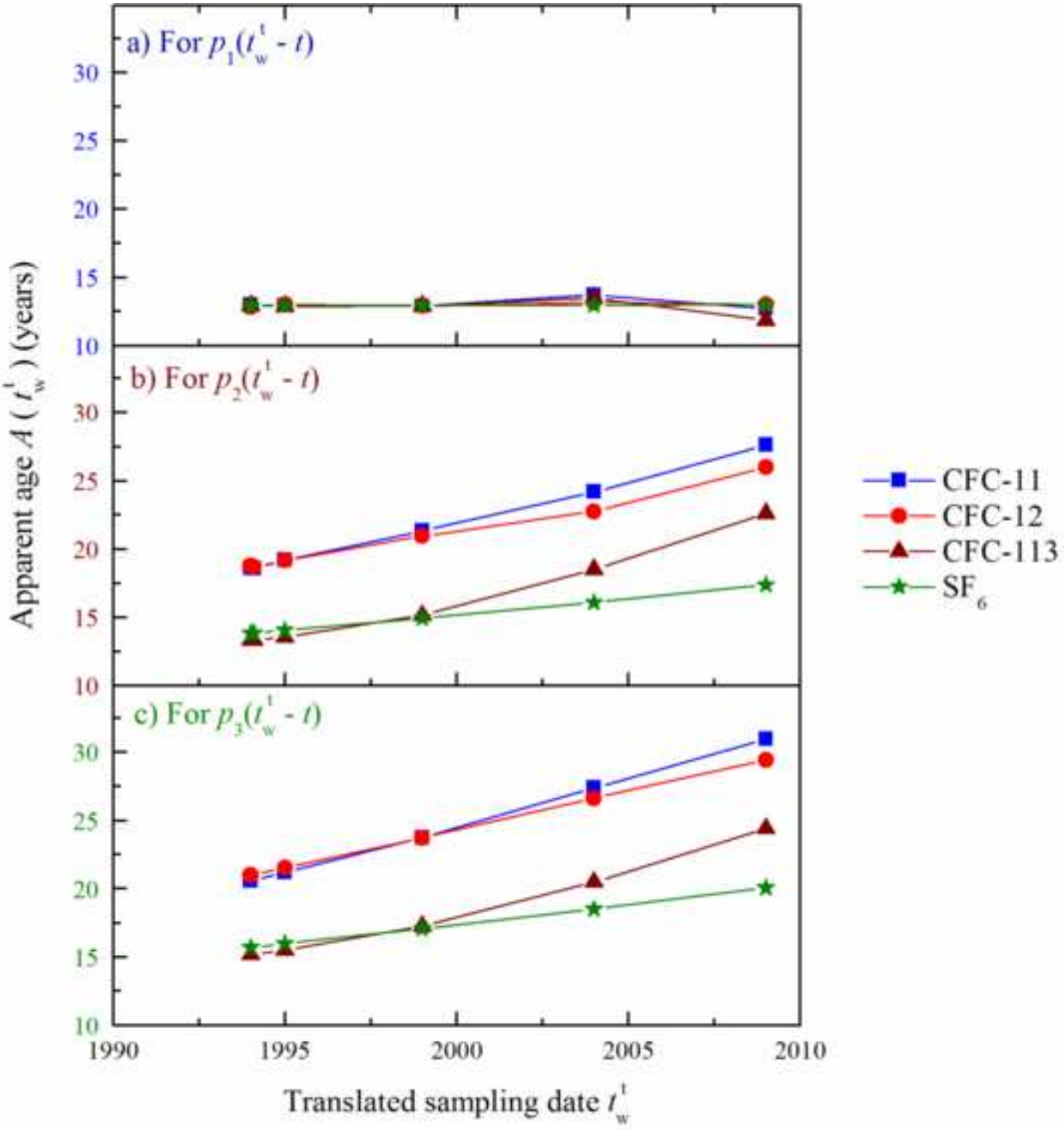

Figure9

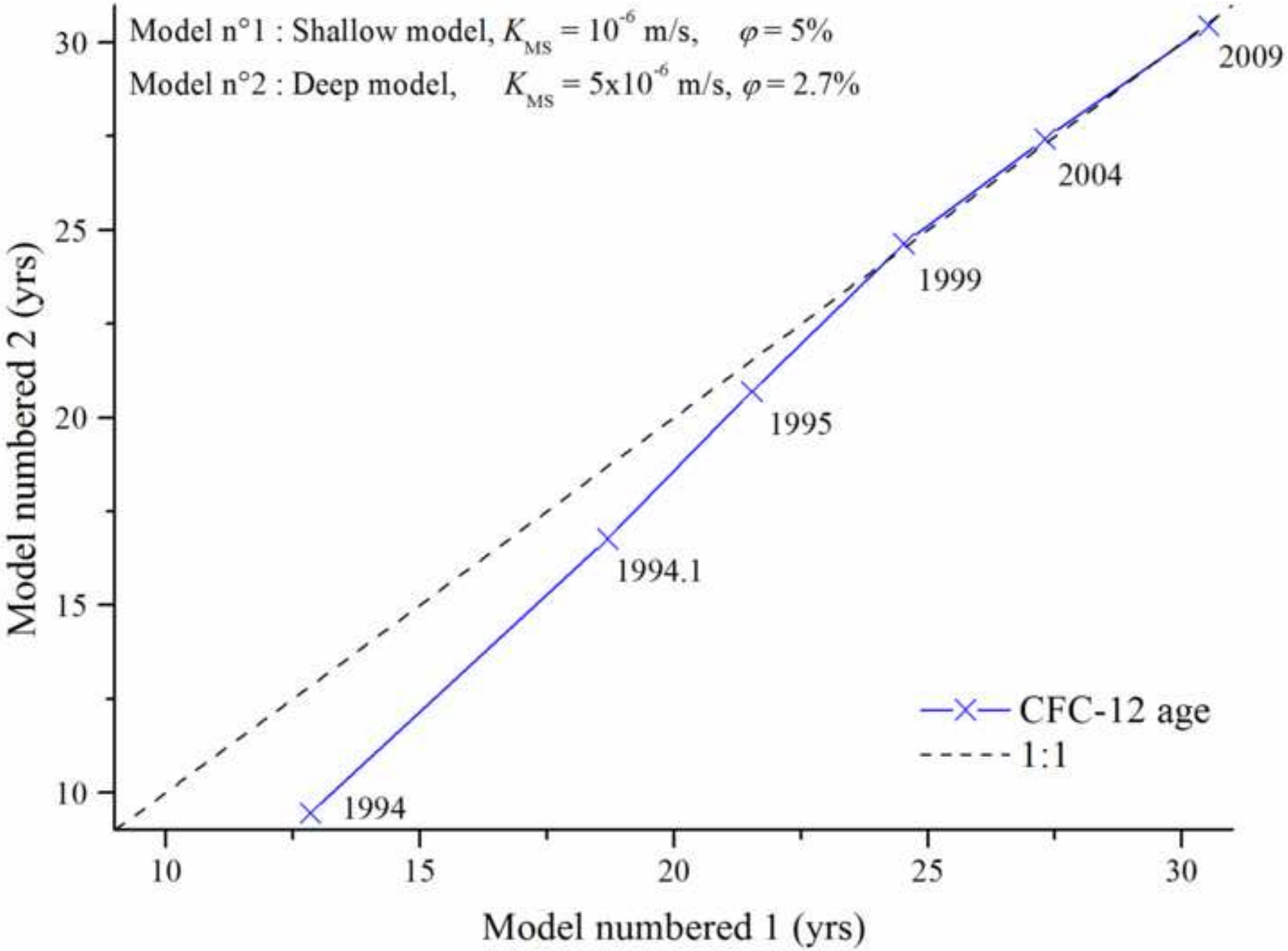

Figure10

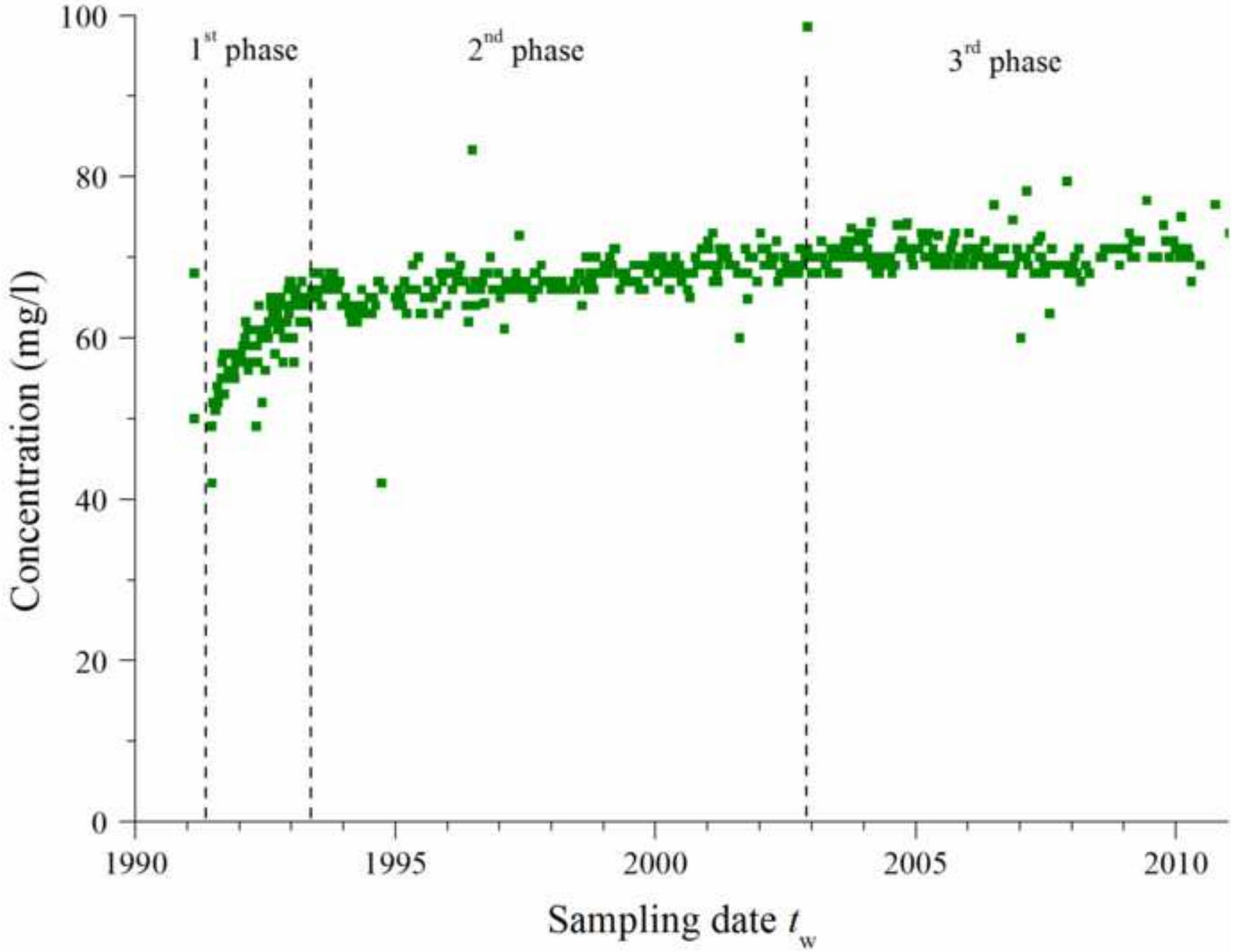

Figure11

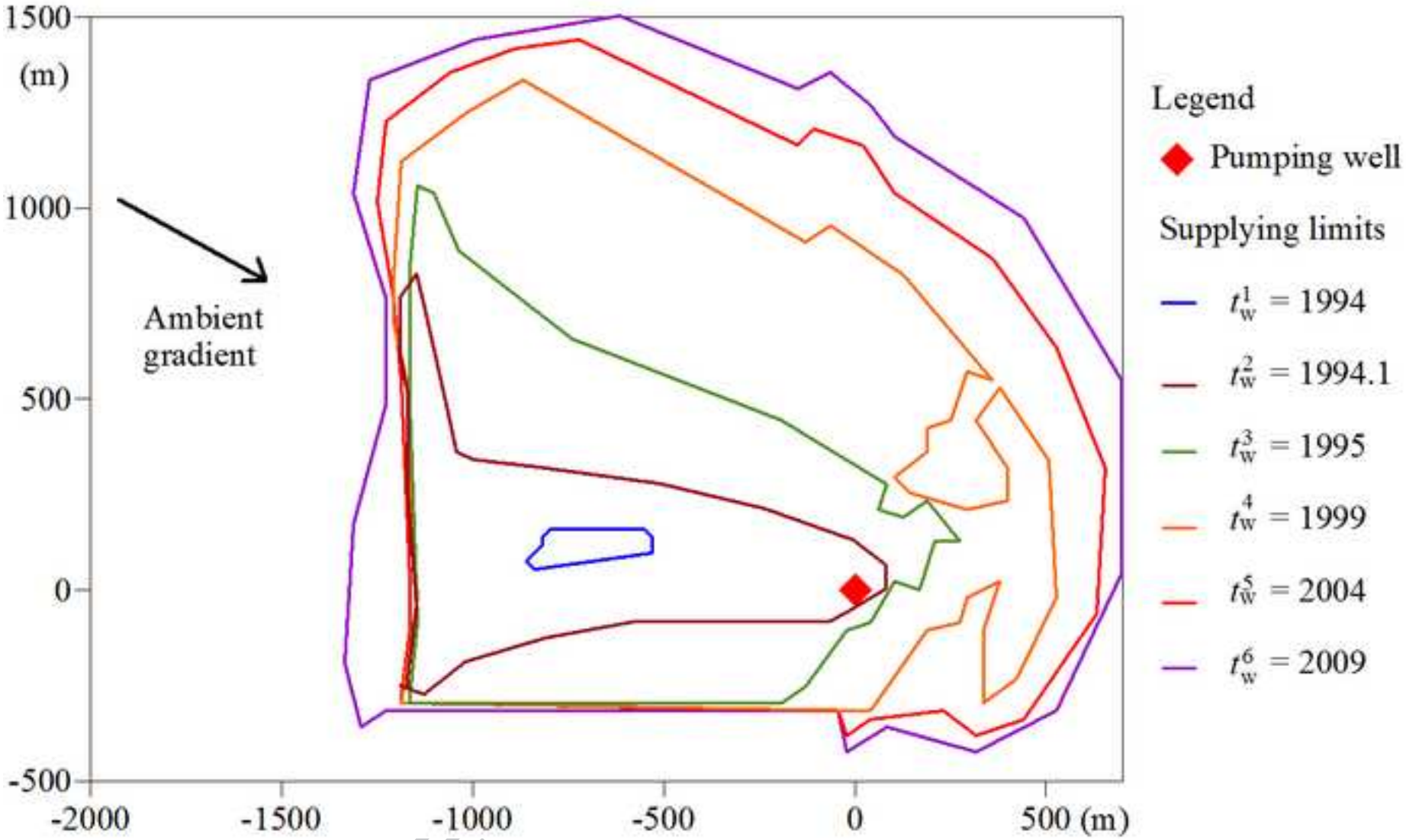

Highlights:

- Pumping start is modeled by an immediate shift between two steady-state flow fields
- Ages deduced from CFCs and SF_6 concentrations evolve in two distinct phases
- Transient flow patterns affect ages just after the pumping start but quickly vanish
- Atmospheric concentrations then transiently weight the residence time distribution
- Similar in terms of magnitude, these two regimes are helpful for models segregation